



Copyright © 2013, Paper 17-024; 51669 words, 14 Figures, 0 Animations, 5 Tables.
<http://EarthInteractions.org>

Toward a Methodology to Investigate the Downstream Flood Hazards on the American River due to Changes in Probable Maximum Flood due to Effects of Artificial Reservoir Size and Land-Use/Land-Cover Patterns

Alfred J. Kalyanapu*

Department of Civil and Environmental Engineering, Tennessee Technological University,
Cookeville, Tennessee

A. K. M. Azad Hossain

National Center for Computational Hydroscience and Engineering, University of
Mississippi, Oxford, Mississippi

Jinwoo Kim

Division of Geodetic Science, School of Earth Sciences, The Ohio State University,
Columbus, Ohio

Wondmagegn Yigzaw and Faisal Hossain

Department of Civil and Environmental Engineering, Tennessee Technological University,
Cookeville, Tennessee

* Corresponding author address: Dr. Alfred J. Kalyanapu, Department of Civil and Environmental Engineering, Tennessee Technological University, 1020 Stadium Drive, Box 5015, Cookeville, TN 38505-0001.

E-mail address: akalyanapu@tntech.edu

C. K. Shum

Division of Geodetic Science, School of Earth Sciences, Ohio State University, Columbus, Ohio, and Institute of Geodesy and Geophysics, Chinese Academy of Sciences, Wuhan, China

Received 30 October 2012; accepted 9 September 2013

ABSTRACT: Recent research in mesoscale hydrology suggests that the size of the reservoirs and the land-use/land-cover (LULC) patterns near them impact the extreme weather [e.g., probable maximum flood (PMF)]. A key question was addressed by W. Yigzaw et al.: How do reservoir size and/or LULC modify extreme flood patterns, specifically PMF via modification of probable maximum precipitation (PMP)? Using the American River watershed (ARW) as a representative example of an impounded watershed with Folsom Dam as the flood control structure, they applied the distributed Variable Infiltration Capacity (VIC) model to simulate the PMF from the atmospheric feedbacks simulated for various LULC scenarios. The current study presents a methodology to extend the impacts of these modified extreme flood patterns on the downstream Sacramento County, California. The research question addressed is, what are the relative effects of downstream flood hazards to population on the American River system under various PMF scenarios for the Folsom Dam? To address this goal, a two-dimensional flood model, the Flood in Two Dimensions–Graphics Processing Unit (Flood2D-GPU), is calibrated using synthetic aperture radar (SAR) and Landsat satellite observations and observed flood stage data. The calibration process emphasized challenges associated with using National Elevation Dataset (NED) digital elevation model (DEM) and topographic light detection and ranging (lidar)–derived DEMs to achieve realistic flood inundation. Following this calibration exercise, the flood model was used to simulate four land-use scenarios (control, predam, reservoir double, and non-irrigation). The flood hazards are quantified as downstream flood hazard zones by estimating flood depths and velocities and its impacts on risk to population using depth–velocity hazard relationships provided by U.S. Bureau of Reclamation (USBR). From the preliminary application of methodology in this study, it is evident from comparing downstream flood hazard that similar trends in PMF comparisons reported by W. Yigzaw et al. were observed. Between the control and nonirrigation, the downstream flood hazard is pronounced by -3.90% for the judgment zone and -2.40% for high hazard zones. Comparing the control and predam scenarios, these differences are amplified, ranging between 0.17% and -1.34% . While there was no change detected in the peak PMF discharges between the control and reservoir-double scenarios, it still yielded an increase in high hazard areas for the latter. Based on this preliminary bottom-up vulnerability assessment study, it is evident that what was observed in PMF comparisons by W. Yigzaw et al. is confirmed in comparisons between control versus predam and control versus nonirrigation. While there was no change detected in the peak PMF discharges between the control and reservoir-double scenarios, it still yielded a noticeable change in the total areal extents: specifically, an increase in high hazard areas for the latter. Continued studies in bottom-up vulnerability assessment of flood hazards will aid in developing suitable mitigation and adaptation options for a much needed resilient urban infrastructure.

KEYWORDS: Floods; Flood2D-GPU; Two-dimensional flood modeling; Flood hazards; Land-use/land-cover change

1. Introduction

The growth and prosperity of human civilization over the centuries resulted in more than 40% of the world's population living within 15 km of rivers (Small and Cohen 2004), dramatically increasing the vulnerability to floods. By 2050, 70% of the world's population is projected to be living in large cities (Cohen 2003). With increasing urbanization and changing patterns of climate and extreme weather (Burby 2001; McCarthy et al. 2001; Montz and Grunfest 2002), understanding flood risk in the vicinity of cities is critical. Improved understanding of flood risk can help the decision makers for practical applications of long-term floodplain planning for cities that are located downstream of critical flood control infrastructure: specifically, flood control dams and artificial reservoirs. These infrastructures are designed to store massive amounts of water to be used for sustenance when demand exceeds natural supply (Hossain et al. 2012). An additional critical role for these dams is the protection of downstream assets against extreme meteorological events such as severe storms and the consequential extreme flooding. Specifically in the continental United States, dams are responsible for hydropower energy (240×10^9 kWh according to 2010 estimates from USEIA 2012); water storage around 1000 million acre-feet (MAF) (Graf 1999); and protecting urban, rural, and other small communities from flood damages. Out of the roughly 84 000 dams in the U.S. National Inventory of Dams, around 16% of the dams are primarily used for controlling floods and thus are located near urban centers and areas (ASDSO 2009).

The downstream flood risks of the dams are dynamic and are affected by various stressors. Specifically, climate impacts and increasing urbanization will lead to increase in magnitude of extreme events (Karl et al. 2009), thus increasing flood risk. Recent research on the presence of dams influencing local, mesoscale, or regional climate (Degu et al. 2011; Hossain et al. 2012) points to the effects of large dams on changing the extreme precipitation patterns such as probable maximum precipitation (PMP). The probable maximum flood (PMF), which is an important factor for hydraulic design of dams, is dependent on PMP and the hydrology of the watershed. A key driver for modification of PMP and PMF during the postdam phase is the land-use/land-cover (LULC) change patterns that are both sensitive to mesoscale weather and surface hydrologic processes. Thus, the very existence of dam could potentially modify the design and operation components that were conceived during the predam phase. This is because future patterns of extreme weather are expected to be different from the past records that were used for the design/operation of dams and for the consequential flood risk assessment of the downstream infrastructure (Hossain et al. 2013).

Generally, the vulnerability assessments performed to study effects of anthropogenic climate change uses a "top down" approach. This method involves using historic hydrology, paleoclimate records, or downscaled climate projections from a global climate model (Burian et al. 2013). However, this vulnerability assessment approach has challenges related to the uncertainties involved in the various scenario generations and the uncertainties introduced in downscaling process (Willems et al. 2011; Burian et al. 2013). Recently, bottom-up approaches, capable of representing high-resolution and site-specific hazard assessments, are being highlighted as an alternative approach to highly uncertainty top-down approaches.

One of these bottom-up approaches was performed by Yigzaw et al. (Yigzaw et al. 2012), where they argued that, since the rainfall–runoff process is a nonlinear process due to the complex interactions of precipitation with the watershed components, a renewed understanding of the influence of LULC changes and the characteristics of reservoirs on the extreme flood patterns is needed. A key question they addressed was, how do reservoir size and/or LULC modify extreme flood patterns, specifically PMF via changes in PMP? They used the American River watershed (ARW) in California as a representative example of an impounded watershed and Folsom Dam as a large artificial reservoir. They applied the distributed Variable Infiltration Capacity (VIC) model to simulate the PMF from the atmospheric feedbacks simulated for various LULC scenarios. They reported that the LULC modification (represented by irrigation) significantly decreased the PMF generation compared to the control condition (2003 LULC condition of the ARW) if there were no irrigation developments in the postdam era. The current study extends these findings from their derived PMF hydrographs and conducts a preliminary vulnerability assessment of these modified extreme flood patterns in terms of flood hazard to downstream population and infrastructure. For more information on procedures to determine the various LULC scenarios, refer to Yigzaw et al. (Yigzaw et al. 2012).

The goal of this research is to perform a bottom-up vulnerability assessment to understand the effects of weather-sensitive LULC change and artificial reservoir size in terms of downstream flood hazard potential to population. The research question addressed is, what are the relative effects on the downstream flood hazards to population on the American River system under various PMF scenarios for the Folsom Dam? To accomplish this objective, a two-dimensional numerical flood model, the Flood in Two Dimensions–Graphics Processing Unit (Flood2D-GPU), is calibrated and used to simulate flood depths and velocities for various PMF simulations. These flood model outputs are compiled into quantifiable downstream flood hazard potential to population using existing flood depth–velocity hazard relationships.

2. Case study

2.1. Folsom Dam and American River watershed

The study uses Folsom Dam and reservoir, which is located in the ARW near the Sierra Nevada mountain range in California (Figure 1). The ARW is mountainous with elevations ranging from 3160 m at the mountains near Sierra Nevada to about 100 m near Folsom Dam. Built in the 1950s by the U.S. Army Corps of Engineers (USACE), the Folsom reservoir collects runoff drained by the 4820 km² of the ARW and serves to protect the urban areas in Sacramento County along the 32-km American River (USBR 1999). With flood control as its primary function, the multipurpose Folsom Dam is a unit of the Central Valley Project (CVP) and is responsible for flood protection for downstream urban areas including the city of Sacramento, which is inhabited by around half a million people and up to quarter million households according to U.S. Census Bureau, 2010, making consequent assessment due to floods crucial. Flooding concerns still remain a major issue for the city of Sacramento ever since the first settlements started in the 1800s. Structural measures like dams and levees (specifically the American River levee system) are the main protection against such floods on the American River.

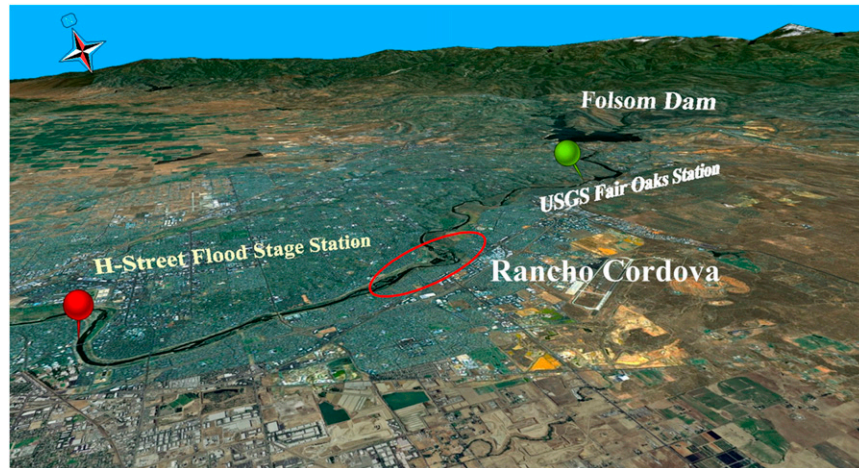


Figure 1. American River case study, downstream of Folsom Dam, California.

2.2. New Year's flood, 1997

In this study, the flood event that occurred during the fall of 1997 is used as a reference event. Referred to as the Great New Year's Flood of 1997, it was one of the largest in the 90-yr Northern California record since 1906. The study area consisted on the river reach starting from the U.S. Geological Survey (USGS) Fair Oaks stream gauge station (gauge 11446500) (USGS Fair Oaks 2012) to the flood stage monitoring station near the H Street Bridge operated by California Department of Water Resources (CA DWR 2012), as shown in Figure 1. The analysis period considered is from 27 December 1996 to 21 January 1997, which included the 1997 catastrophic Sacramento flood event.

The National Elevation Dataset (NED) digital elevation model (DEM) was used to represent topography and was downloaded from the USGS Seamless Server (now through <http://nationalmap.gov/>). Additionally, highly detailed lidar topography data for the study area were obtained from the city of Sacramento, and a DEM at 32-m spatial resolution was generated in ArcGIS environment. An average Manning's surface roughness was estimated by interpreting available observed data (including existing cross sections, levee locations, and levee elevations) using existing data provided by the Sacramento Flood Control Agency (SAFCA) and the California Department of Water Resources Flood Management Division. The flow hydrograph for the 1997 flood event was obtained from the archived USGS data for the USGS Fair Oaks station (Figure 2).

For the flood event, observed flood stages at the H Street flood stage monitoring station are obtained from California Data Exchange Center (see Figure 3) are used. Additionally, spatially observed data derived from the synthetic aperture radar (SAR) and Landsat satellite data are also gathered. More details on processing and usage of satellite data are presented in section 3.2.

2.3. Relevance of case study to this study

Two major flood events occurred in the recent past in 1986 and 1997 in Sacramento. These two floods have prompted engineers of the USACE to reevaluate

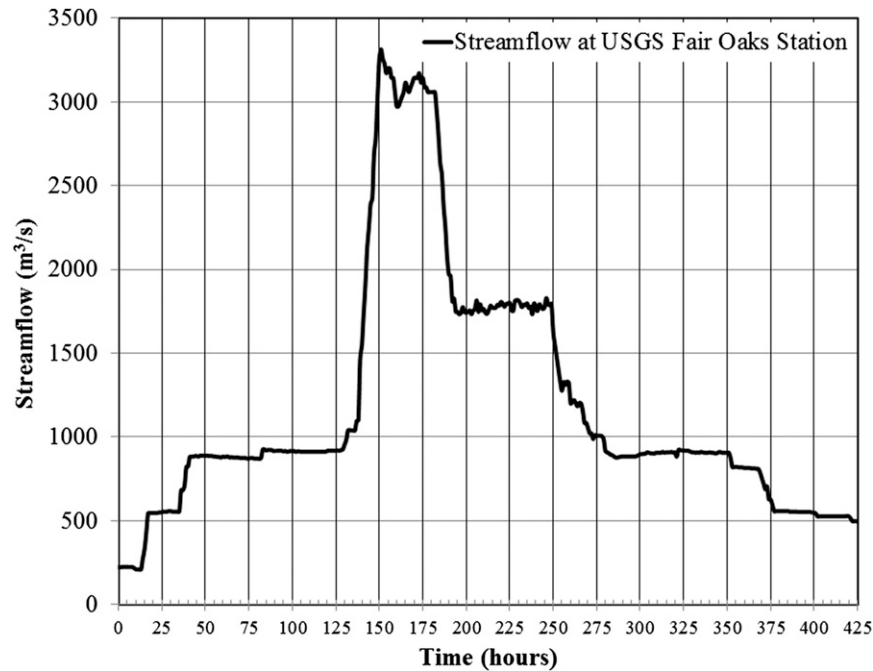


Figure 2. Observed streamflow at USGS Fair Oaks station.

the flood frequency analysis of Folsom Dam from a 500-yr recurrence interval (0.2% annual exceedance probability) to a 70-yr recurrence interval ($\sim 1.4\%$ annual exceedance probability) in 1998 (NRC 1999). In fact, there are a number of floods that occurred prior to systematic streamflow measurement practices that began in 1905 (Ohara et al. 2011). The revised flood frequency analysis has shown that the Sacramento levees, in their current form, are likely unable to withstand the new 100-yr flood (1% annual exceedance probability event) (NRC 1999). In this context, research is conducted to understand the impacts of dams on changing the precipitation patterns suggesting incorporating the local, mesoscale, or regional climate impact of reservoirs in dam design and their operation (Degu et al. 2011; Hossain et al. 2012; Yigzaw et al. 2012). This preliminary study extends the previous study by Yigzaw et al. (Yigzaw et al. 2012) and quantifies the estimated PMFs in terms of downstream flood hazards to population downstream of Folsom Dam on the American River.

2.4. Multiple PMF scenarios from previous research

Yigzaw et al. (Yigzaw et al. 2012) investigated the impact of modification of PMP on PMF due to changes in dam-driven LULC and reservoir size for Folsom Dam on the ARW. They applied the distributed VIC model (Liang et al. 1994) to simulate the PMF from the atmospheric feedbacks simulated for various LULC scenarios. The scenarios considered were predam, control, reservoir double, and nonirrigation. The readers are referred to Yigzaw et al. (Yigzaw et al. 2012) for information on PMF development process. The hydrologic model (VIC) used for these simulations was calibrated using measured streamflow data at Fair Oaks station (Figure 1).

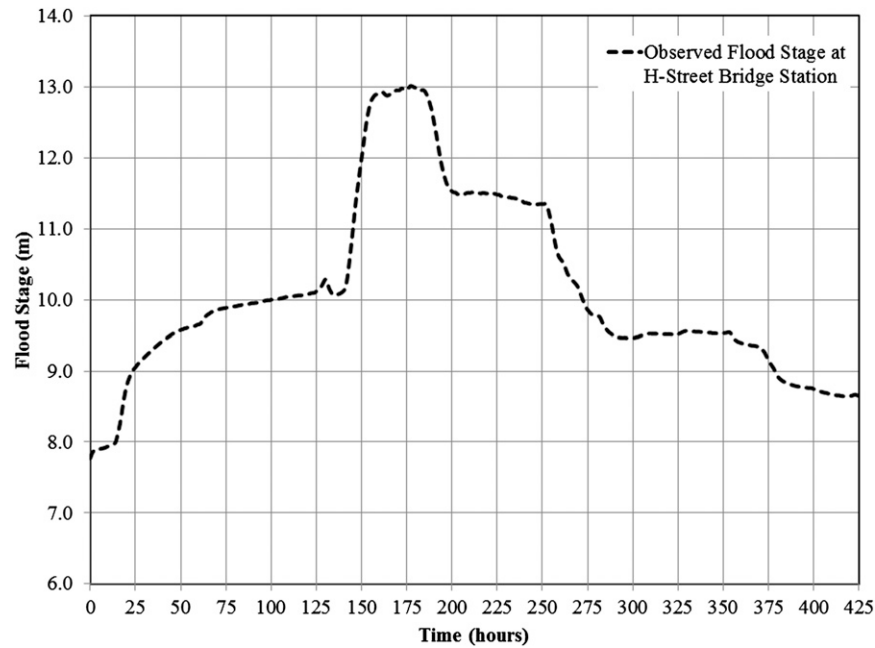


Figure 3. Observed flood stage at the H Street Bridge station.

This paragraph briefly summarizes the results from Yigzaw et al. (Yigzaw et al. 2012). From their analysis, Yigzaw et al. (Yigzaw et al. 2012) determined that control scenario resulted in a smaller PMF peak flood (about $105 \text{ m}^3 \text{ s}^{-1}$) compared to the predam scenario because of a decrease in simulated PMPs in the upstream ARW after the Folsom Dam construction (Figure 4). The comparison of PMF hydrographs between the control scenario and the reservoir-double scenario representing the impact of different reservoir size with no change in LULC did not yield any difference in terms of peak discharge, even though changes in 72-h total PMP values were identified in a previous study by Woldemichael et al. (Woldemichael et al. 2012). Comparison of the control scenario PMF with the nonirrigation scenario showed that the PMF peak discharge decreased (about $125 \text{ m}^3 \text{ s}^{-1}$) when irrigation was not considered. This is because the absence of enhanced evapotranspiration due to nonirrigation decreased the potential maximum precipitation, thus reducing the peak discharge. Table 1 lists the main conclusions from their PMF comparisons. Note that there was no noticeable change in times to peak. The current study uses the flow hydrographs to drive a flood model and determine resultant flood risk to perform bottom-up vulnerability assessment.

3. Methodology

3.1. Two-dimensional flood model

For simulating downstream flood hazards in terms of spatially varied flood depths and velocities, a two-dimensional (2D) flood model called Flood2D-GPU is applied (Kalyanapu et al. 2011). The Flood2D-GPU is an unsteady numerical

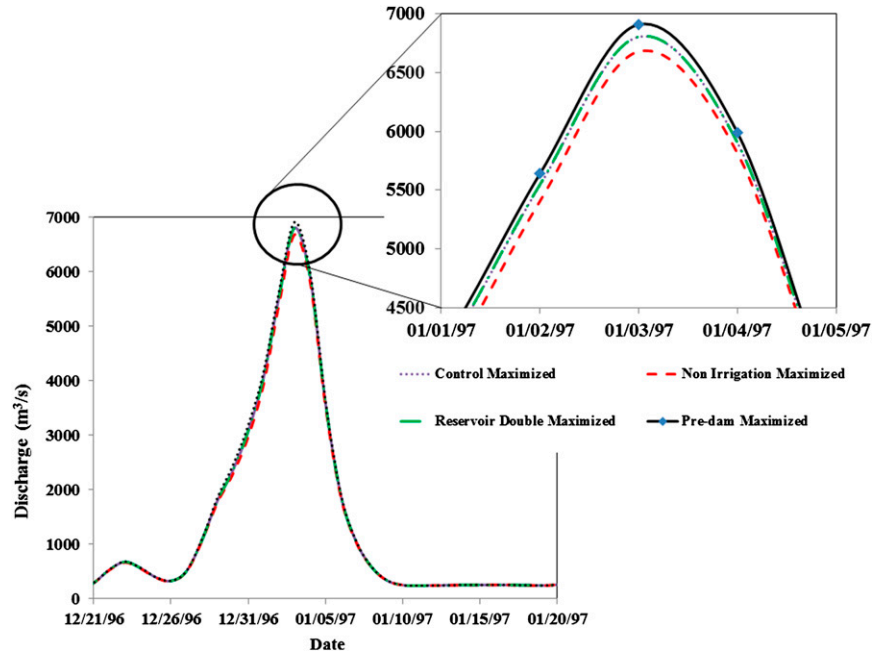


Figure 4. Simulated PMF hydrographs for LULC-driven PMP scenarios. Note that the term “maximized” refers to PMP-derived flows.

flood model solving the nonlinear hyperbolic shallow water equations using a first-order accurate upwind difference scheme (Patankar 1980; Ferziger and Perić 2002). A staggered grid stencil is used to define the computational domain with the water depth h in the center of the cell and u and v velocities on the cell edges. The future model time step is constrained using the Courant condition. It is programmed using the Graphics Processing Unit (GPU) framework developed in Nvidia’s Compute Unified Development Architecture (CUDA) and has been shown to decrease the computational time by up to two orders of magnitude. The model has been used in various applications including river flooding, dam break simulations, population at risk studies, and flood damage estimation (Kalyanapu et al. 2011; Kalyanapu et al. 2012; Kalyanapu et al. 2013, manuscript submitted to *J. Flood Risk Manage.*).

The principal dataset for Flood2D-GPU is topographic data (i.e., DEM). The numerical solution is computed on a uniform grid to take advantage of the use of downloadable DEM data. While using an irregular mesh is efficient for model computing, the advantage of using the DEM is that its extent is the entire

Table 1. Comparison of PMF peak discharges for multiple scenarios relative to the control scenario.

Scenario	Change in peak discharge
Predam	$105 \text{ m}^3 \text{ s}^{-1}$
Reservoir double	0
Nonirrigation	$-125 \text{ m}^3 \text{ s}^{-1}$

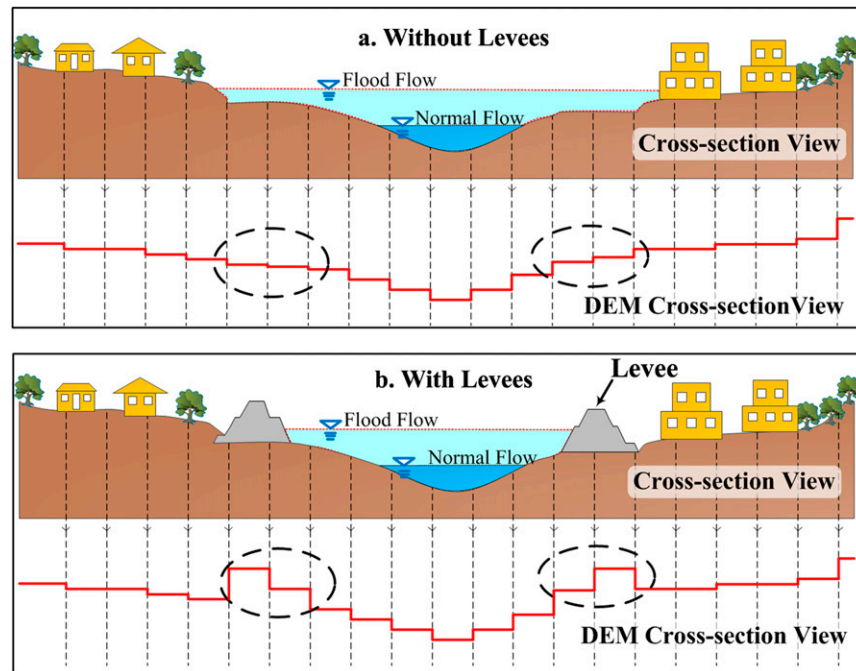


Figure 5. Geometric representation of levees in Flood2D-GPU modeling domain. The cross-sectional view represents the natural river and floodplain cross section, and the DEM cross-sectional view with red line represents the DEM elevation values used by the model.

computational domain and no preprocessing step is required to generate a computational mesh permitting flood model applications to meet time constraints. Additional data needed for the model includes a surface roughness coefficient (Manning’s n value) and flow hydrograph. Currently, the roughness of the entire domain is represented using a single Manning’s n value in 2D modeling applications (Hunter et al. 2007; Kalyanapu et al. 2011). This assumption is justified for this study as literature indicates that the Manning’s roughness coefficient not only represents the roughness of the surface but also the turbulent momentum losses along with compensating the assumptions of depth-averaged flows (Werner et al. 2005; Fabio et al. 2010). A “bulk” Manning’s n value representing the dominant land use may be used as a starting point for a calibration exercise consequently estimating a calibrated single Manning’s surface roughness coefficient for the case study (Werner et al. 2005). Future versions of the Flood2D-GPU model will include options to include a spatial variation of Manning’s n values using an appropriate raster dataset [e.g., National Land Cover Dataset (NLCD) from USGS] and it is outside the scope of this study. The flow hydrograph is another input dataset that can be developed from a hydrologic model, dam break model, or observations. The source location of the input hydrograph must be defined. When simulating floods in urban areas, Flood2D-GPU can represent the geometric features such as levees on the DEM by GIS-based preprocessing. Figure 5 presents a schematic view of artificially “burning” (i.e., after GIS-based preprocessing) the levees along the

river (Figure 5b) to realistically represent the floods in the floodplain. To represent levees, the elevation values of the cells containing these features are increased by the equivalent height of the levee. Not including these levees in the topography will lead to increased flooding and exaggerated flood extent as represented in Figure 5a.

3.2. Calibration of Flood2D-GPU

To implement the Flood2D-GPU model for flood hazard quantification, it is calibrated for the American River using the January 1997 flood event. The calibration procedure is performed in two parts. First, the lidar DEM was modified by adjusting the main channel bathymetry and raising levee heights along the American River. This is because the DEMs were not accurately representing the fluvial bathymetry and American River levee system. This resulted in exaggerated flood depths and inundation extents (e.g., Figure 5a). Second, after adjusting the DEMs, the Flood2D-GPU model is calibrated for Manning's n by iteratively changing the parameter value and comparing the simulated flood extent and flood stages with the observed data. To estimate the performance of the flood simulation, two different metrics were used. The first metric used is to compare the simulated flood stages to the observed flood stage at the H Street Bridge, obtained from the California Data Exchange Center (Figure 3).

Second, the spatial extent of the flood inundation from the model simulation was verified by comparing with observed flood inundation extent. The observed flood inundation extent was developed through remote sensing analyses of European Remote Sensing Satellite (ERS) SAR scenes (obtained on 4 January 1997), *Radarsat-1* SAR imageries (obtained on 8, 15, and 17 January 1997), and the *Landsat-5* Thematic Mapper imagery (acquired on 14 January 1997). This section briefly explains the remote sensing analysis performed on these satellite imageries to generate observed flood inundation extents. The observed peak discharge at the USGS Fair Oaks station was $3313 \text{ m}^3 \text{ s}^{-1}$ around 0700 local time (LT) 2 January 1997. Satellite imagery during the peak flow was not available for the American River, and the closest possible imagery available is from 4 January 1997, at which time peak discharge already passed through the river and the discharge at the station reduced to 45% of the peak discharge.

The satellite imageries were processed by applying the iterative self-organizing data analysis technique (ISODATA) clustering algorithm (Jensen 2007; Lillesand and Kiefer 2000) and density slicing technique (Campbell 2002; Hossain et al. 2009) and by classifying areas as water and nonwater to separate the areas occupied by different water bodies in the study site. The ISODATA clustering algorithm was applied on the optical imagery (*Landsat-5* TM data) and density slicing technique was applied on the microwave imagery (*Radarsat-1* SAR and ERS SAR data). The areas covered by water bodies (e.g., channel water and other permanent water bodies in the flood plains) in the dry season were subtracted from the areas covered by water bodies in the wet season to derive the flooded areas in the given time. In this study, *Landsat-5* TM imagery acquired in July 1996 was used to extract the location and extent of the dry season water bodies.

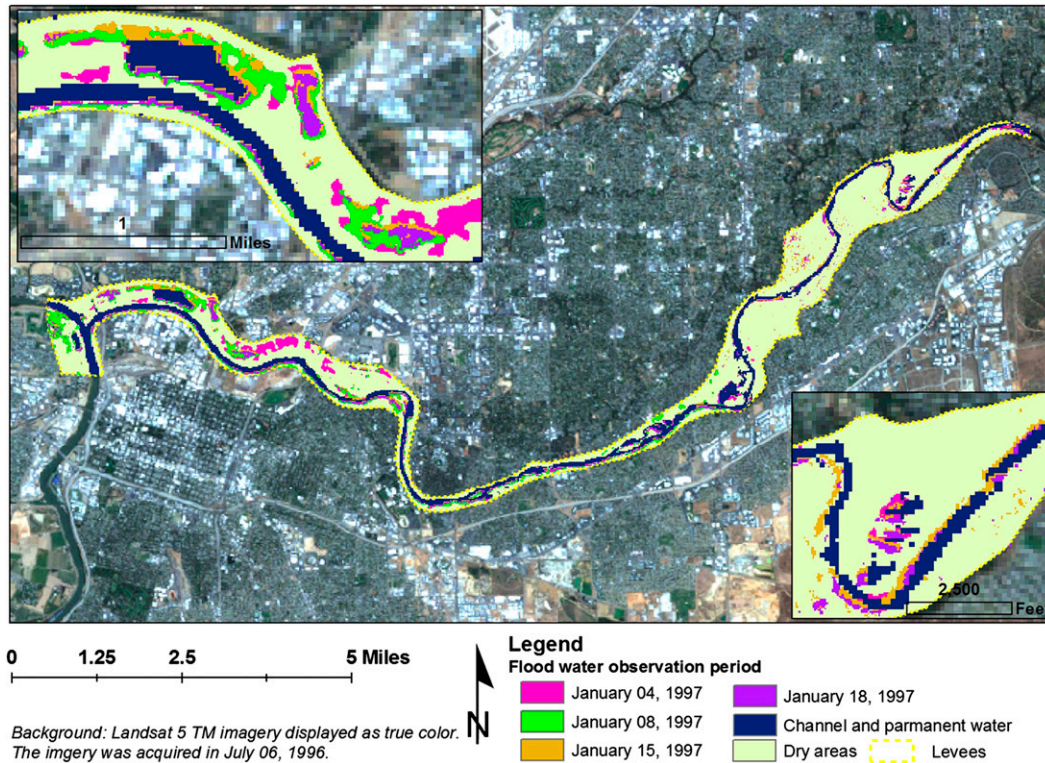


Figure 6. Observed flood inundation after performing remote sensing analysis on the four satellite imageries.

Figure 6 shows the multitemporal satellite imagery depicting the flood water dynamics of the New Year's flood event. It is observed that there was no flooding beyond the American River flood control levees as the peak flood during this event $3313 \text{ m}^3 \text{ s}^{-1}$ was less than the peak carrying capacity of the American River levees. The results from the calibration process are further explained in section 4.1.

3.3. Quantification of flood hazard

The flood hazard from various PMF scenarios is quantified in terms of downstream hazard to populations using the hazard classifications provided from ACER (ACER 1988). This technical report published by the U.S. Bureau of Reclamation (USBR) has been widely used to provide guidelines for dam safety hazard classification. From a collection of curves provided in this report, a depth–velocity hazard relationship corresponding to permanent residences and commercial and public buildings is employed (Figure 7). The flood hazard level is classified as low-danger, judgment, and high-danger zones. For each grid cell in the low-danger zone, the possible lives in jeopardy are assumed to be zero. In the high-danger zone, lives in jeopardy are assumed to be 100% of the total population in the grid

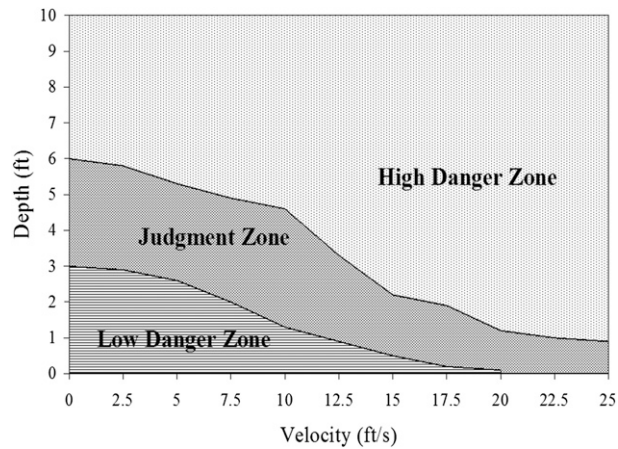


Figure 7. Flood depth–flow velocity hazard classification diagram for flood hazard classification (source: ACER 1988).

cell. The judgment zone represents a zone where the lives in jeopardy are considered to be variable between 0% and 100% and it is up to the analyst to use engineering judgment (ACER 1988).

4. Results and discussion

4.1. New Year's flood event calibration

The initial Flood2D-GPU simulations were performed using the NED DEM (at 32-m spatial resolution) downloaded from USGS. The 32-m spatial resolution was chosen because the simulation of the flow hydrographs corresponds to a total duration of 18 days as represented in Figure 2. The computational domain consisted of 32 000 grid cells at this spatial resolution; it took approximately 9.2 trillion calculations on each grid cell to route the flow hydrograph (29 million numerical iterations were performed at each grid cell). The computational runtime for simulating this hydrograph was 10 h. Additionally, the model simulations resulted in significant amounts of output files [180 different output files for every time step with a total of 2 gigabytes (GB) for every simulation] containing simulated flood depths and velocities.

4.1.1. DEM adjustment

The DEMs were modified by adjusting the main channel bathymetry and raising levee heights along the American River. This is because the DEMs from NED and derived from lidar were not accurately representing the fluvial bathymetry and American River levee system and simulated exaggerated flood depths and inundation extents (see Figures 8 and 9) while no significant flooding was reported on the American River (see Figure 6). This DEM adjustment allowed Flood2D-GPU to simulate flood depths closer to the observed flood depths at H Street Bridge.

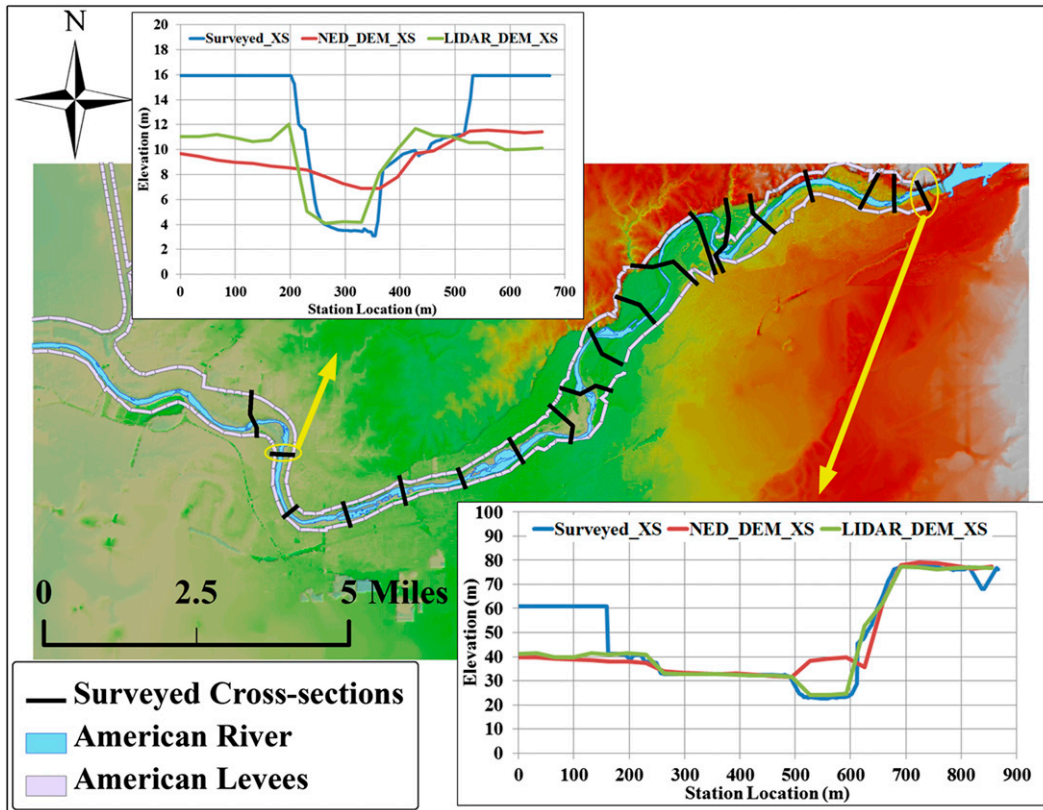


Figure 8. Comparison of cross sections derived from NED and lidar DEMs with surveyed cross sections.

Additionally, a relatively closer match of simulated flood inundation extent to observed extent was observed.

This overestimation is due to the limitations of the NED in representing the channel and floodplain bathymetry. Prior research on DEMs indicates that NED-derived DEMs have smoother elevations thus overestimating flood inundation (Sanders 2007). It was also determined through evaluation in the GIS environment that the NED and lidar DEMs did not adequately represent the presence of levees along with the fact that the spatial resolution is 32 m, thus smoothing the elevations within the grid cells that contain the levees. Figure 8 visually depicts the errors in the cross sections derived from NED and lidar DEMs when compared to the surveyed cross sections. Analyzing 19 different locations along the American River with observed surveyed cross-sectional data, it was found that the root-mean-square error (RMSE) estimated using Equation (1) ranged between 1.74 and 11.75 m for NED DEM. For the lidar DEM, RMSE decreased because of better topographic representation and ranged between 1.3 and 9.1 m. This error is mainly due to the inability of NED and lidar DEMs to represent the levees (Figure 8). Thus, only the lidar-derived DEM acquired from the city of Sacramento were used as the primary DEM data at 32-m spatial resolution,

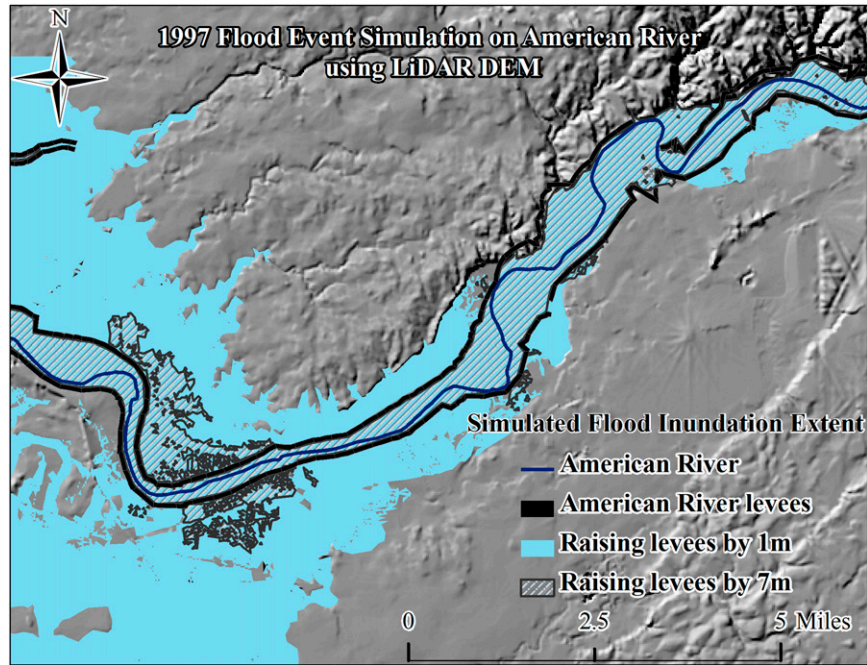


Figure 9. Simulated flood inundation extents using lidar DEM and raising levee heights.

$$\text{RMSE} = \sqrt{\frac{1}{n} \sum_{i=1}^n (\varepsilon_i)^2}, \quad (1)$$

where n is the number of cross-sectional points and ε is the difference between the observed and simulated elevation values.

Another study by Quadros et al. (Quadros et al. 2008) suggests that topographic lidar cannot penetrate water surface; hence, depending on date of data acquisition and corresponding flow conditions in nearby water bodies, the channel bathymetry will not be accurately integrated. To represent the channel bathymetry along with the representing the levee features in the DEM topography, for the calibration of Flood2D-GPU model for the 1997 event, the following modifications to the topography data were performed and the simulations were tested:

- (i) The levees along the American River are added into the lidar DEM by raising the elevations in the corresponding grid cells by the observed levee elevations.
- (ii) The main channel of the American River was artificially “burned” (or deepened) to increase the conveyance in the main channel to avoid the accumulated flood waters to spill over into the floodplain.

After several iterations of adjusting the levee heights and burning the DEMs, it was observed that, when the levee heights are raised to 7 m at selected locations (near

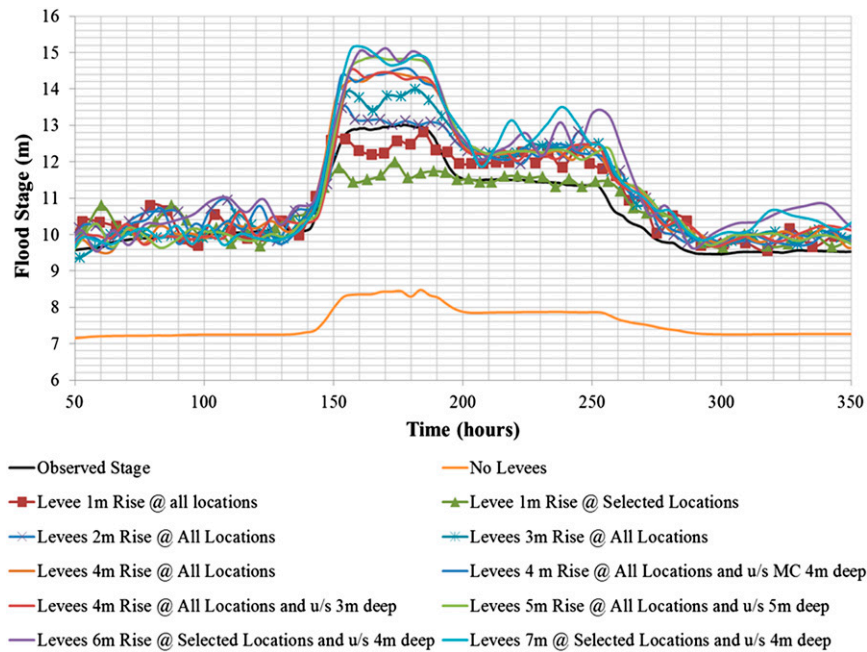


Figure 10. Variation in the simulated flood depths under various combinations of levee height increases and DEM burning compared to observed flood stage (time period from 29 Dec 1996 to 10 Jan 1997).

the Rancho Cordova neighborhood in the lower American River; refer to Figure 1), the flood was contained within the levees as observed in Figure 6.

These effects of DEM modifications on the model results were tested by comparing the simulated flood depths at the H Street gauge. Figure 10 presents the comparison of the simulated flood depths from all the above-mentioned scenarios to the observed flood stage at the H Street flood gauge station. It is observed from Figure 10 that Flood2D-GPU significantly underestimated (by 35% around 2 January 1997) during the peak flood stage at the H Street flood gauge, when the levees were not raised. This underprediction was because of the combination of “flat” topographic representation from the DEM and because of the significant artificial flooding due to spillage that allowed lower amounts of flood water to reach the flood gauge. This spillage was contained within the levees by artificially raising the levee elevations by 7 m. However, it resulted in overprediction of the flood stage by 16.37% on 2 January 1997. Table 2 presents the comparison of the simulated flood stage with the observed flood extent and the times to peak.

A few additional modifications to the levee heights and channel bottom did not yield significantly different simulations, so they are not included in this study. Additional modifications will also increase the amount of computational resources required to simulate the flood event. For example, to simulate 450 h of flood stage and corresponding simulation, Flood2D-GPU simulations required approximately 5.4 h of computational time. This is a “better than real-time” computational achievement, in line with what was previously reported in Kalyanapu et al. (Kalanapu et al. 2011;

Table 2. Comparison of simulated peak flood stage and time to peak T_p for various levee heights and upstream main channel depth adjustments (observed peak flood stage is 13.01 m at 175 h).

Description	Relative difference in flood inundation (km ²)	Peak stage (m)	Percentage difference in stage	T_p (h)	Percentage difference in T_p
No Levees	—	8.48	−34.84	184	4.91
Levee 1-m rise	64.5	12.81	−1.57	185	5.71
Levee 2-m rise	65.0	13.48	3.60	153	−12.57
Levee 4-m rise	38.2	14.44	10.94	172	−1.71
Levee 4-m rise and upstream section 4 m deep	39.5	14.55	11.77	180	2.86
Levee 5-m rise and upstream section 4 m deep	25.7	14.88	14.29	166	−5.14
Levee 7-m rise and upstream section 4 m deep	20.0	15.15	16.37	162	−7.43

Kalyanapu et al. 2012). However, significant storage space of 10.9 GB was also required for each of these above listed simulations, which included a total of 11 982 generated files of various formats [e.g., Environmental Systems Research Institute (ESRI) GRID, text files, and ASCII files]. This is roughly equivalent to more than 10 000 books according to Wynn (Wynn 2012). Thus, these above listed artificial adjustments of the levee heights and main channel bottom elevations were considered as all possible calibration options of topographic data for this American River case study.

This DEM adjustment exercise highlighted the difficulty in accurately representing the surface topography that significantly influenced the model simulations. There is still a considerable amount of research effort needed to investigate the errors caused due to DEM and improving their topographic representation for accurate flood predictions. With improved ways to account for channel bathymetry and identification of surface structures like the American River levee system in this research, realistic flood simulation will be possible.

4.1.2. Calibration of Manning’s roughness

Using the adjusted DEM, Flood2D-GPU is calibrated to estimate appropriate Manning’s surface roughness. The current version of Flood2D-GPU uses a single representative Manning’s n value for the flood modeling domain to simulate downstream flood extent. Future versions of the model will include options to include spatially variable Manning’s n values into models, and it is outside the scope of this study. Automated calibration techniques were not implemented for calibration in this study due to the significant computational demand. To calibrate the model for Manning’s n , 12 values of Manning’s n range between 0.013 (representing concrete surfaces) and 0.6 (a higher value of Manning’s n is used here to include the bulk effects such as energy losses and lateral momentum transfers). The simulated flood depths and flood inundation extents are compared to observed flood stage at H Street Bridge station and observed flood extent, respectively (Table 3). To estimate the Manning’s n value resulting in the simulations closer to observe results, three statistics including RMSE [Equation (1)], bias, and cumulative relative error (CRE) are used [Equations (2) and (3) below] to compare observed and

Table 3. Summary of Manning's n calibration results.

Manning's n	Stage			Inundation extent Relative difference (km ²)
	RMSE (m)	Bias (m)	CRE (m)	
0.013	0.90	-0.79	0.07	12.6
0.04	0.64	0.11	0.05	14.0
0.1	1.07	0.75	0.08	28.4
0.15	1.70	1.34	0.13	61.4
0.2	2.23	1.89	0.18	77.9
0.25	2.62	2.27	0.22	97.4
0.3	3.10	2.66	0.27	123.6
0.35	3.50	2.92	0.31	131.9
0.4	3.93	3.10	0.34	138.2
0.45	4.31	3.21	0.38	143.1
0.5	4.50	3.28	0.39	148.9
0.6	4.95	3.24	0.43	164.2

simulated flood stage. By comparing these multiple simulations, a Manning's n value of 0.04 from the initial range that minimized these errors was selected based on these statistics. It was used in the development of flood risk maps for the four PMF scenarios presented by Yigzaw et al. (Yigzaw et al. 2012),

$$\text{Bias} = \frac{1}{n} \sum_{i=1}^n \varepsilon_i \quad \text{and} \quad (2)$$

$$\text{CRE} = \frac{\frac{1}{n} \sum_{i=1}^n |\varepsilon_i|}{\frac{1}{n} \sum_{i=1}^n (\text{OBS}_i)}, \quad (3)$$

where n is the number of data points in the stage hydrograph, ε is the difference between the observed and simulated stage values, and OBS is the observed stage.

4.2. Application of PMFs (modified through PMP from LULC changes in postdam era)

This section presents the simulated results of Flood2D-GPU model in terms of downstream flood hazards to population based on the four PMFs scenarios (refer to section 2.2), to investigate the effects of LULC and artificial reservoir size. The PMFs for the four scenarios control, predam, reservoir double, and nonirrigation were provided as flow inputs to the model. The DEM corresponding to raising the levees by 7 m and burning the upstream section of the American River by 4 m was used based on the process described in section 3.2. The simulated flood depths and velocities from the model are translated to flood hazard estimates in terms of downstream flood hazard to population estimates by applying the flood risk framework presented in Kalyanapu et al. (Kalyanapu et al. 2012) and using the

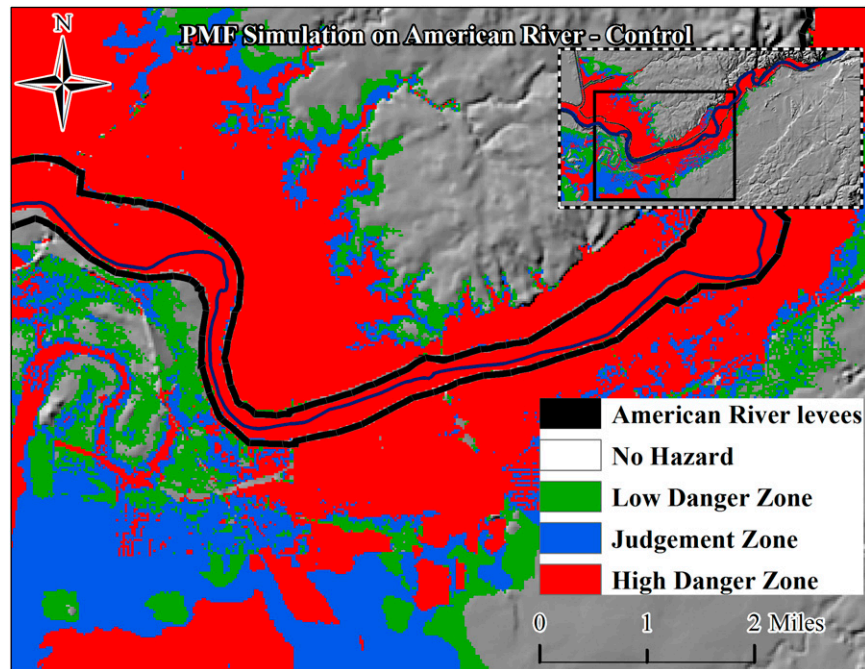


Figure 11. Simulated flood hazard map for the control maximized condition. Inset shows full extent.

depth–velocity hazard classification curve provided by ACER (ACER 1988) (Figure 7).

Figures 11–14 show the flood hazard simulated for the control, predam, reservoir-double, and nonirrigation PMF scenarios. Tables 4 and 5 summarize the areal extent of each of the flood hazard for the four scenarios and percent difference estimates relative to the control scenario, respectively. The high areal extent for the no-hazard zone is due to the presence of nonflooded areas in the chosen computational domain. It is observed that, for all the four PMF scenarios, the areal extents of high hazard zone are found to be larger compared to the low hazard and judgment zone. This is understandable because PMF hydrograph is indicative of the maximum possible runoff conditions from the probable maximum precipitation (PMP) (USBR 1987), representing the “worst case scenario” and justifiably so used in the design of large hydraulic structures (McCuen 1998).

Yigzaw et al. (Yigzaw et al. 2012) concluded that the peak flow from the control PMF scenario was higher than the nonirrigation PMF scenario by about 1.8%. The estimated percent relative differences (–3.90% and –2.40% for judgment and high hazard zones, respectively) confirm the reported pattern with much pronounced response in magnitude, when the analysis is extended to downstream flood hazard. They also reported that the control PMF was simulated to have lesser peak discharge than predam PMF, about 1.5%. These differences are dampened when downstream flood hazards are estimated, ranging between 0.47% and –1.34% for the judgment and high hazard zones, respectively. While there was no change

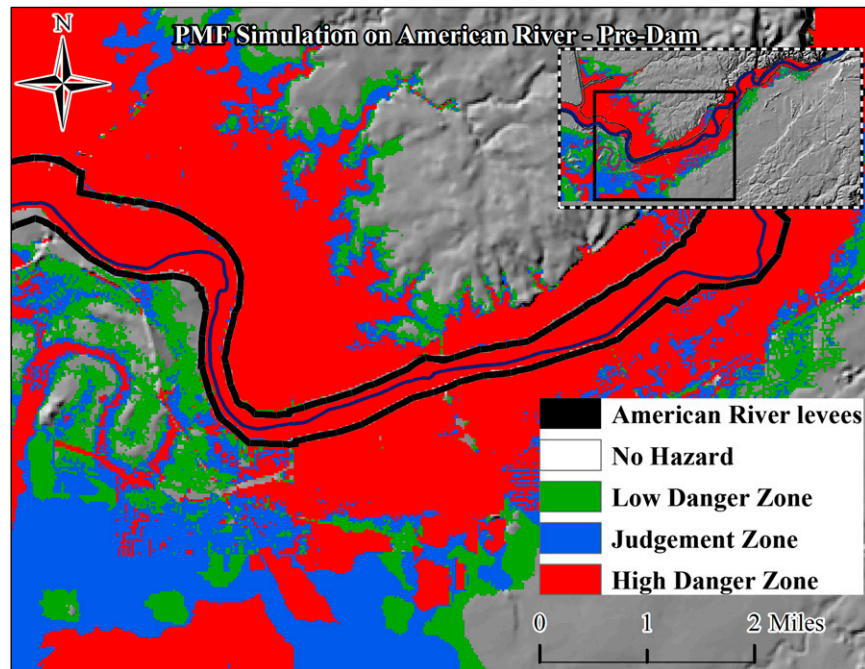


Figure 12. Simulated flood hazard map for the predam condition.

detected in the peak PMF discharges between the control and reservoir-double scenarios, it still yielded a noticeable change in the total areal extents of the flood hazards. Table 4 indicates that the control scenario resulted in high hazard areas that are more than the reservoir-double scenario by -3.32% in the high hazard zones. These influences on downstream flood hazard estimation are not only due to the magnitudes of peak discharge but also due to the shape of hydrograph and the total flood volume (area under the hydrograph).

The magnitudes of difference in hazard areas noticed from Tables 4 and 5 may be smaller, but these changes are significant when potential population affected is considered. For instance, the city of Sacramento, which lies within the current study area, has a population density of 1861 people per square kilometer (according to <http://quickfacts.census.gov>). So, a difference of 1.8 km^2 of high hazard area between the nonirrigation and control scenarios will result in the possible difference in population prone to high flood hazard of approximately 3350. These four PMF scenarios exhibit significant differences when the downstream flood hazards are considered. Thus, by considering this bottom-up vulnerability assessment and including the various LULC-driven changes, a more actionable map may be provided to decision makers.

Additional investigations into the influence of the additional flood characteristics along with the peak PMF discharge are needed to increase understanding on the impacts on downstream flood hazards and is beyond the scope of this preliminary study. There is additional need for investigating methods to improve the topography by adjusting DEMs and reducing the elevation discrepancies that will improve the study of the robustness of the flood hazard estimations. This is a

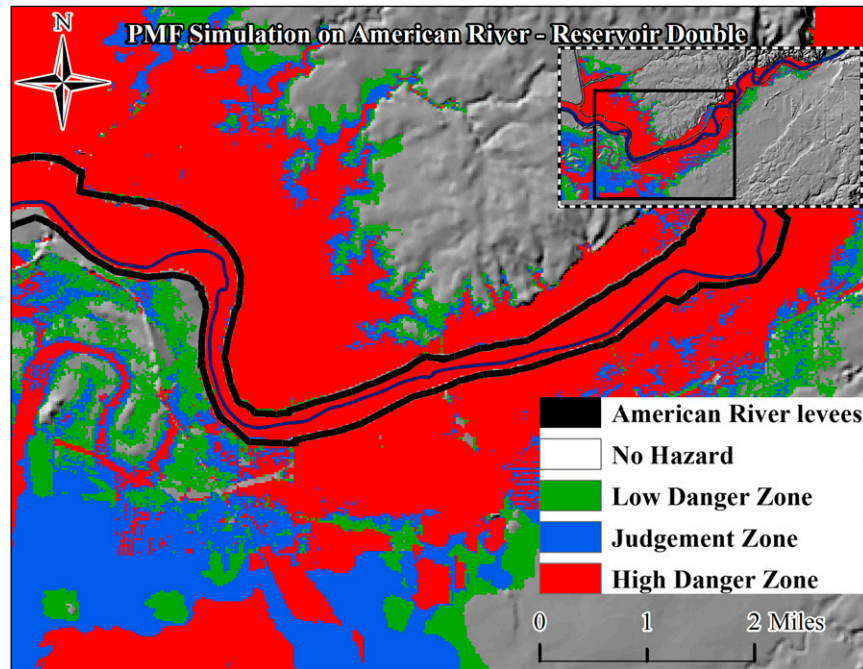


Figure 13. Simulated flood hazard map for the dam-double condition.

preliminary study that used computationally intensive high-resolution dynamic flood modeling along with a suite of hydrologic and atmospheric models (Woldemichael et al. 2012; Yigzaw et al. 2012). Additional improvements such as including multiple flood events, investigating the effects of model parameters (e.g., surface roughness), integrating advanced digital image processing techniques (Hossain et al. 2009), and performing probabilistic flood risk estimations (Kalyanapu et al. 2012) will improve the reliability of the high-resolution bottom-up flood hazard assessments.

5. Summary and conclusions

The current study presents a methodology to extend the findings of Yigzaw et al. (Yigzaw et al. 2012) and incorporates the effects of land use/land cover and artificial reservoir size in terms of downstream flood hazard potential to population. The research question addressed is, what are the relative effects downstream flood hazards to population on the American River system under various PMF scenarios for Folsom Dam? To accomplish this objective, a two-dimensional numerical flood model, Flood2D-GPU, is calibrated and used to simulate flood depths and velocities for various PMF simulations in the American River watershed. The calibration process highlighted the topographic representation issues associated with NED DEM and topographic lidar-derived DEMs. The model was calibrated by using observed flood stage and by using spatial inundation extent–derived SAR and Landsat satellite observations. Lidar-derived DEM adjusted by raising levees by 7 m near the Rancho

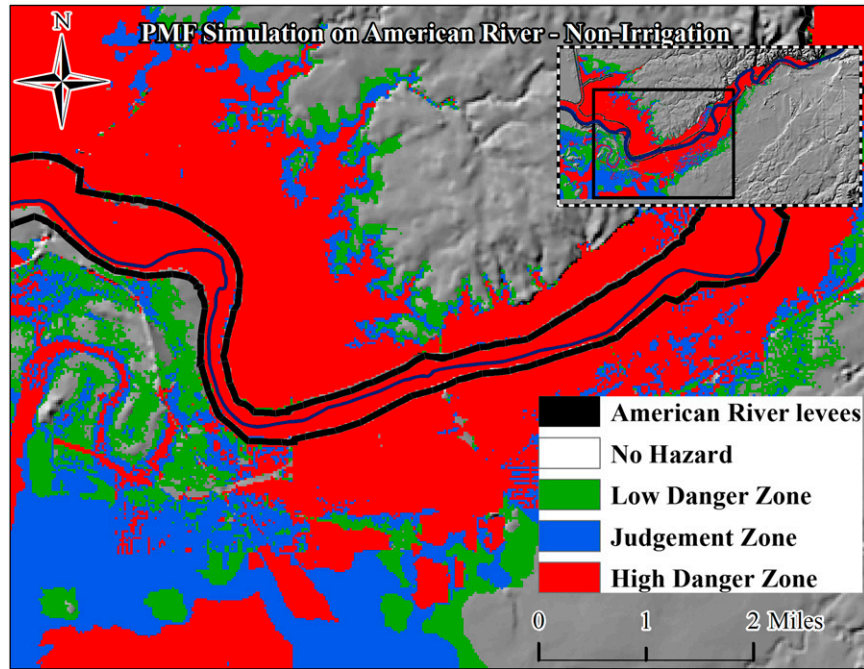


Figure 14. Simulated flood hazard map for the nonirrigation condition.

Cardova region and the upstream section of American River deepened by 4 m, which resulted in a closer match of simulated flood depths and flood extent with the observed data. The calibrated flood model was used to simulate four PMF scenarios (control, predam, reservoir double, and nonirrigation). These flood model outputs are compiled into quantifiable downstream flood hazard potential to population using existing flood depth–velocity hazard relationships. Based on this preliminary bottom-up vulnerability assessment study, it is evident from comparing downstream flood hazard that what was observed in PMF comparisons by Yigzaw et al. (Yigzaw et al. 2012) was confirmed in comparisons between the control versus predam and the control versus nonirrigation. Between the control and nonirrigation, the downstream flood hazard is pronounced (−3.90% and −2.40% for judgment and high hazard zones, respectively), especially for the judgment and high hazard zones. Comparing the control and predam scenarios, no significant differences were observed in the resulting flood hazards. While there was no change detected in the peak PMF discharges between the control and reservoir-double scenarios, it still

Table 4. Simulated flood hazard areas for the four PMF scenarios.

Scenario	Flood hazard area (km ²)			
	No hazard	Low hazard	Judgment	High hazard
Control	212.3	27.2	33.1	74
Nonirrigation	216.9	25.6	31.8	72.2
Reservoir double	217.5	25.6	31.9	71.5
Predam	213.2	27.2	33.2	73

Table 5. Percent relative difference in simulated flood hazard areas for the three PMF scenarios compared to the control scenario.

Scenario	Relative difference in area (%)			
	No hazard	Low hazard	Judgment	High hazard
Nonirrigation	2.17	−5.68	−3.90	−2.40
Reservoir double	2.48	−5.80	−3.72	−3.32
Predam	0.41	0.20	0.17	−1.34

yielded a noticeable change in the total areal extents, specifically increase in high hazard areas for the latter. This is a preliminary study of extending the reservoir and LULC-driven PMF results into quantifiable flood risk to population. While no clear correlations in flood hazards for these PMFs were observed, this study indicates the need for more investigations into the effects of LULC and reservoir size on the downstream vulnerability. Future studies on investigating influences of other flood characteristics along with the peak PMF discharge, including additional case study events to replicate these findings and explicitly considering the uncertainties involved in the hydrologic, hydraulic, and flood risk mapping processes, will provide improved understanding of this bottom-up vulnerability assessment and aid in developing suitable mitigation and adaptation options for a much needed resilient urban infrastructure.

Acknowledgments. The authors acknowledge the technical support and data received from Sacramento Area Flood Control Agency (SAFCA), Sacramento County GIS, California Department of Water Resources–Flood Management, and MBK Engineers. The Ohio State University component of the research is partially funded by USGS (Grant G10AC00628; Dr. John W. Jones) and by Ohio State University’s Climate, Water and Carbon Program (<http://cwc.osu.edu>).

References

- ACER, 1988: Downstream hazard classification guidelines. Assistant Commissioner—Engineering and Research Tech. Memo. 11, 56 pp.
- ASDSO, 2009: The cost of rehabilitating our nation’s dams—A methodology, estimate and proposed funding mechanisms. Association of Dam Safety Officials Task Committee Rep., 52 pp.
- Burby, R. J., 2001: Flood insurance and floodplain management: The US experience. *Environ. Hazards*, **3**, 111–122.
- Burian, S. J., T. Walsh, A. J. Kalyanapu, and S. G. Larsen, 2013: Climate Vulnerabilities and adaptation of urban water infrastructure systems. *Climate Vulnerability: Understanding and Addressing Threats to Essential Resources*, R. A. Pielke Sr., Ed., Elsevier, 87–107.
- CA DWR, cited 2012: California Data Exchange Center. [Available online at http://cdec.water.ca.gov/cgi-progs/selectQuery?station_id=HST.]
- Campbell, J. B., 2002: *Introduction to Remote Sensing*. 3rd ed. Taylor and Francis, 621 pp.
- Cohen, E. J., 2003: Human population: The next half century. *Science*, **302**, 1172–1175, doi:10.1126/science.1088665.
- Degu, A. M., F. Hossain, D. Niyogi, R. A. Pielke Sr., J. M. Shepherd, N. Voisin, and T. Chronis, 2011: The influence of large dams on surrounding climate and precipitation patterns. *Geophys. Res. Lett.*, **38**, L04405, doi:10.1029/2010GL046482.

- Fabio, P., G. T. Aronica, and H. Apel, 2010: Towards automatic calibration of 2D flood propagation models. *Hydrol. Earth Syst. Sci.*, **14**, 911–924.
- Ferziger, J. H., and M. Perić, 2002: *Computational Methods for Fluid Dynamics*. 3rd ed. Springer, 423 pp.
- Graf, W. L., 1999: Dam nation: A geographic census of American dams and their large-scale hydrologic impacts. *Water Resour. Res.*, **35**, 1305–1311.
- Hossain, A., Y. Jia, and X. Chao, 2009: Validation of CCHE2D model using digital image processing techniques and satellite imagery. *Proc. 33rd IAHR Biennial Congress*, Vancouver, BC, Canada, International Association of Hydraulic Engineering and Research, 3156–3163.
- Hossain, F., A. M. Degu, W. Yigzaw, S. Burian, D. Niyogi, J. M. Shepherd, and R. Pielke Sr., 2012: Climate feedback-based considerations to dam design, operations and water management in the 21st century. *ASCE J. Hydrol. Eng.*, **17**, 837–850, doi:10.1061/(ASCE)HE.1943-5584.0000541.
- , A. T. Woldemichael, A. Degu, W. Yigzaw, C. Mitra, and J. M. Shepherd, 2013: Water resources vulnerability in the context of rapid urbanization of Dhaka City (a South Asian mega city). *Climate Vulnerability: Understanding Threats to Water Resources*, Elsevier, 393–404.
- Hunter, N. M., P. D. Bates, M. S. Horritt, and M. D. Wilson, 2007: Simple spatially distributed models for predicting flood inundation: A review. *Geomorphology*, **90**, 208–225.
- Jensen, J. R., 2007. *Remote Sensing of the Environment: An Earth Resource Perspective*. 2nd ed. Prentice Hall, 592 pp.
- Kalyanapu, A. J., S. Shankar, E. R. Pardyjak, D. R. Judi, and S. J. Burian, 2011: Assessment of GPU computational enhancement to a 2D flood model. *Environ. Modell. Softw.*, **26**, 1009–1016.
- , D. R. Judi, T. N. McPherson, and S. J. Burian, 2012: Monte Carlo-based flood modelling framework for estimating probability weighted flood risk. *J. Flood Risk Manage.*, **5**, 37–48.
- Karl, T. R., J. M. Melillo, and T. C. Peterson, Eds., 2009: *Global Climate Change Impacts in the United States*. Cambridge University Press, 188 pp.
- Liang, X., D. P. Lettenmaier, E. F. Wood, and S. J. Burges, 1994: A Simple hydrologically based model of land surface water and energy fluxes for GSMs. *J. Geophys. Res.*, **99** (D7), 14 415–14 428.
- Lillesand, T. M., and R. W. Kiefer, 2000. *Remote Sensing and Image Interpretation*. 4th ed. John Wiley and Sons, 724 pp.
- McCarthy, J. J., O. F. Canziani, N. A. Leary, D. J. Dokken, and K. S. White, Eds., 2001: *Climate Change 2001: Impacts, Adaptation and Vulnerability*. Cambridge University Press, 976 pp.
- McCuen, R. H., 1998: *Hydrologic Analysis and Design*. Prentice-Hall, 859 pp.
- Montz, B. E., and E. Grunfest, 2002: Flash flood mitigation: Recommendations for research and applications. *Environ. Hazards*, **4**, 15–22.
- NRC, 1999: *Improving American River Flood Frequency Analyses*. National Academies Press, 113 pp.
- Ohara, N., M. L. Kavvas, S. Kure, Z. Q. Chen, S. Jang, and E. Tan, 2011: A physically based estimation of maximum precipitation over American River watershed, California. *J. Hydrol. Eng.*, **16**, 351–361, doi:10.1061/(ASCE)HE.1943-5584.0000324.
- Patankar, S. V., 1980: *Numerical Heat Transfer and Fluid Flow*. Taylor and Francis, 197 pp.
- Quadros, N. D., P. A. Collier, and C. S. Fraser, 2008: Integration of bathymetric and topographic lidar: A preliminary investigation. *Int. Arch. Photogramm. Remote Sens. Spat. Inf. Sci.*, **37**, 1299–1304.
- Sanders, B., 2007: Evaluation of on-line DEMs for flood inundation modeling. *Adv. Water Resour.*, **30**, 1831–1843.
- Small, C., and J. Cohen, 2004: Continental physiography, climate, and the global distribution of human population. *Curr. Anthropol.*, **54**, 269.
- USBR, 1987: Design of small dams. U.S. Bureau of Reclamations Water Resources Tech. Publ., 904 pp.

- , 1999: Hydraulic model study of Folsom Dam spillway performance and Stilling basin abrasion. U.S. Bureau of Reclamations Water Resources Research Laboratory Rep. R-99-08, 55 pp.
- USEIA, cited 2012: Electricity explained—Electricity in the United States. [Available online at http://www.eia.gov/energyexplained/index.cfm?page=electricity_in_the_united_states.]
- USGS Fair Oaks, cited 2012: USGS 11446500 American R a Fair Oaks CA. [Available online at http://waterdata.usgs.gov/ca/nwis/inventory/?site_no=11446500&agency_cd=USGS&.]
- Werner, M. G. F., N. M. Hunter, and P. D. Bates, 2005: Identifiability of distributed floodplain roughness values in flood extent estimation. *J. Hydrol.*, **314**, 139–157.
- Willems, P., K. Arnbjerg-Nielsen, J. Olsson, and V. T. V. Nguyen, 2011: Climate change impact assessment on urban rainfall extremes and urban drainage: Methods and shortcomings. *Atmos. Res.*, **103**, 106–118.
- Woldemichael, A. T., F. Hossain, R. A. Pielke Sr., and A. Beltrán-Przekurat, 2012: Understanding the impact of dam-triggered land-use/land-cover change on the modification of extreme precipitation. *Water Resour. Res.*, **48**, W09547, doi:10.1029/2011WR011684.
- Wynn, L. S., cited 2012: How much text is in a kilobyte or megabyte? 22 February 2011, wiseGEEK. [Available online at <http://www.wisegeek.com/how-much-text-is-in-a-kilobyte-or-megabyte.htm>.]
- Yigzaw, W., F. Hossain, and A. Kalyanapu, 2012: Impact of artificial reservoir size and land use/land cover patterns on probable maximum precipitation and flood: The case of Folsom Dam on American River. *J. Hydrol. Eng.*, **18**, 1180–1190, doi:10.1061/(ASCE)HE.1943-5584.0000722.

Earth Interactions is published jointly by the American Meteorological Society, the American Geophysical Union, and the Association of American Geographers. Permission to use figures, tables, and *brief* excerpts from this journal in scientific and educational works is hereby granted provided that the source is acknowledged. Any use of material in this journal that is determined to be “fair use” under Section 107 or that satisfies the conditions specified in Section 108 of the U.S. Copyright Law (17 USC, as revised by P.L. 94-553) does not require the publishers’ permission. For permission for any other from of copying, contact one of the copublishing societies.
